

Article

Selective CW Laser Synthesis of MoS₂ and Mixture of MoS₂ and MoO₂ from (NH₄)₂MoS₄ Film

Noah Hurley¹, Bhojraj Bhandari¹, Steve Kamau¹, Roberto Gonzalez Rodriguez¹ , Brian Squires¹, Anupama B. Kaul^{2,3} , Jingbiao Cui¹ and Yuankun Lin^{1,3,*} 

¹ Department of Physics, University of North Texas, Denton, TX 76203, USA; noahhurley@my.unt.edu (N.H.); bhojrajbhandari@my.unt.edu (B.B.); stevekamau@my.unt.edu (S.K.); roberto.gonzalezrodriguez@unt.edu (R.G.R.); brian.squires@unt.edu (B.S.); jingbiao.cui@unt.edu (J.C.)

² Department of Materials Science and Engineering, University of North Texas, Denton, TX 76203, USA; anupama.kaul@unt.edu

³ Department of Electrical Engineering, University of North Texas, Denton, TX 76203, USA

* Correspondence: yuankun.lin@unt.edu; Tel.: +1-940-565-4548

Abstract: Very recently, the synthesis of 2D MoS₂ and WS₂ through pulsed laser-directed thermolysis can achieve wafer-scale and large-area structures, in ambient conditions. In this paper, we report the synthesis of MoS₂ and MoS₂ oxides from (NH₄)₂MoS₄ film using a visible continuous-wave (CW) laser at 532 nm, instead of the infrared pulsed laser for the laser-directed thermolysis. The (NH₄)₂MoS₄ film is prepared by dissolving its crystal powder in DI water, sonicating the solution, and dip-coating onto a glass slide. We observed a laser intensity threshold for the laser synthesis of MoS₂, however, it occurred in a narrow laser intensity range. Above that range, a mixture of MoS₂ and MoO₂ is formed, which can be used for a memristor device, as demonstrated by other research groups. We did not observe a mixture of MoS₂ and MoO₃ in the laser thermolysis of (NH₄)₂MoS₄. The laser synthesis of MoS₂ in a line pattern is also achieved through laser scanning. Due to the ease of CW beam steering and the fine control of laser intensities, this study can lead toward the CW laser-directed thermolysis of (NH₄)₂MoS₄ film for the fast, non-vacuum, patternable, and wafer-scale synthesis of 2D MoS₂.



Citation: Hurley, N.; Bhandari, B.; Kamau, S.; Gonzalez Rodriguez, R.; Squires, B.; Kaul, A.B.; Cui, J.; Lin, Y. Selective CW Laser Synthesis of MoS₂ and Mixture of MoS₂ and MoO₂ from (NH₄)₂MoS₄ Film. *Micromachines* **2024**, *15*, 258. <https://doi.org/10.3390/mi15020258>

Academic Editor: Hugo Aguas

Received: 16 January 2024

Revised: 4 February 2024

Accepted: 7 February 2024

Published: 9 February 2024



Copyright: © 2024 by the authors. Licensee MDPI, Basel, Switzerland. This article is an open access article distributed under the terms and conditions of the Creative Commons Attribution (CC BY) license (<https://creativecommons.org/licenses/by/4.0/>).

Keywords: laser material processing; MoS₂; (NH₄)₂MoS₄; laser synthesis; laser direct writing; laser-directed thermolysis; Raman; photoluminescence; nanopattern; thermal annealing

1. Introduction

Since the mono-layer graphene was demonstrated through exfoliation in 2004 [1], two-dimensional (2D) materials have been one of the hot research topics in the field of chemistry, physics, and electronics for their applications in future sensors, transistors, memristors, and single-photon emitters [2–13]. At the same time, researchers started the synthesis of large-area 2D materials and developed the chemical vapor deposition (CVD) method [14]. Currently, the 2D materials from the family of transition-metal dichalcogenide [3,15–18] are targeted for developing next-generation electronic materials due to their unique properties such as direct or indirect band gap modulation and quantum confinement. Large-area thin films of transition-metal dichalcogenide can be fabricated via CVD [17,19]. However, the CVD-based synthesis is limited by the requirement of long processing time and high temperatures (≈ 1000 °C).

In the micro/nano-fabrication field, the solution-based material process is economically favored because it can start with a spin-coating of wafer-scale films, is compatible with existing CMOS micro/nano-fabrication processes, can be integrated onto various functional substrates, and is especially scalable at low cost and with rapid synthesis [19]. High-quality MoS₂ or WS₂ films have been achieved using a single-source precursor such as ammonium tetrathiomolybdate (ATM) (NH₄)₂MoS₄ or (NH₄)₂WS₄, respectively, through thermolysis

for electronic devices applications [20,21]. The thermogravimetric analyzer (TGA) curve for $(\text{NH}_4)_2\text{MoS}_4$ has shown a possible conversion pathway of $(\text{NH}_4)_2\text{MoS}_4$ to MoS_2 [22]. In the temperature range of 150–330 °C, there is an initial conversion of $(\text{NH}_4)_2\text{MoS}_4$ to MoS_3 , and then decomposition of the intermediate MoS_3 to MoS_2 in the temperature range of 380–500 °C [22]. Although $(\text{NH}_4)_2\text{MoS}_4$ can be dissolved in DI water, the formed film quality is poor. Through the mixing of $(\text{NH}_4)_2\text{MoS}_4$ precursor with a polymer matrix polyethyleneimine (PEI), a high quality $(\text{NH}_4)_2\text{MoS}_4$ can be prepared, leading to MoS_2 on a 6-inch SiO_2/Si wafer [23,24]. Very recently, a laser synthesis of MoS_2 and WS_2 through the pulsed laser ($\lambda = 1.06 \mu\text{m}$, pulse duration $\sim 100 \text{ ps}$)-directed thermolysis in ambient conditions has achieved wafer-scale samples and devices [2,23,25].

Laser direct writing cannot only generate 2D and 3D patterns for a top-down process, but also generate atomic layer material such as graphene or nanowires for bottom-up nanofabrication [26–28]. It can also generate desired patterns and atomic layers of MoS_2 [29]. CW laser has a long coherent length and the holographic interference of CW laser beams can form large area 2D or 3D patterns [30–32]. It is exciting to have the laser synthesis of atomic layered materials, such as MoS_2 using CW laser, and simultaneously in large-area patterns formed through the interference of CW laser beams. Although pure MoS_2 is useful, the mixture of MoS_2 and its oxide has been used in memristor devices [13].

In this paper, we are able to realize visible CW laser-directed thermolysis of $(\text{NH}_4)_2\text{MoS}_4$ for the formation of MoS_2 , instead of the infrared pulsed laser. We study the laser intensity-dependent thermolysis of $(\text{NH}_4)_2\text{MoS}_4$ and the formation of MoS_2 and oxide. The threshold laser power for the laser synthesis of MoS_2 is clearly observed although the operation window for the laser synthesis of MoS_2 is narrow. We also compare the laser synthesis process with thermal annealing.

2. Sample Preparation and Measurement Methods

A 2D layered MoS_2 was mechanically exfoliated from the bulk sample with a thickness larger than 300 nm. Ammonium tetrathiomolybdate $(\text{NH}_4)_2\text{MoS}_4$ (99.95%, Thermo Scientific Chemicals, Waltham, MA, USA) was used as it is (i.e., crystals) or prepared as a film. It has a melting point of 300 °C. Preparation of ammonium tetrathiomolybdate film on a glass slide followed the instructions given by the procedure document. A low concentration of ammonium tetrathiomolybdate is desired with less than 0.1 wt%. We mixed 0.1 g of $(\text{NH}_4)_2\text{MoS}_4$ crystal powder with DI water [33] and then sonicated it for 20 min. The solution is then hydrothermally heated in water for three hours at 95 °C. In this study, we focus on whether we can achieve the laser synthesis of MoS_2 from $(\text{NH}_4)_2\text{MoS}_4$ and pay attention to the film quality in future research. We drop coated the ATM solution onto glass slides and then dried them at room temperature. Once dry, slides are then exposed to laser light of 532 nm and examined via Raman spectroscopy simultaneously.

Raman and photoluminescence (PL) spectra were measured with a Renishaw inVia Raman Microscope that is equipped with a 532 nm laser with a controllable power by software. A grating of 1800 lines/mm was used for the Raman and PL measurements. A 50 \times objective lens (numerical aperture NA = 0.5) was used for all measurements. The exposure time was 1 s for Raman and 20 s (also 5 accumulations to improve the signal/noise ratio) for the PL unless specified otherwise. The laser spot size is 20.8 microns when using a 50 \times objective lens, as measured in another paper [18]. Thus, a laser power of 0.3 mW corresponds to laser intensities of 0.176 kWcm^{-2} . Because the setting of laser power is in a simple digital of 0.3, 0.4, 0.5, etc., we leave the plot in the x -axis in power (mW) instead of laser intensity.

A line pattern of MoS_2 is formed through the laser thermolysis of $(\text{NH}_4)_2\text{MoS}_4$. For a certain film sample and exposure range, we initially performed Raman measurement with increasing laser power and discovered a laser power threshold for the formation of MoS_2 . Using Raman mapping for a line (a grid of 1×50 , for example) and a laser power above the laser power threshold, the laser scanned through the $(\text{NH}_4)_2\text{MoS}_4$ film at a rate of 1 micron per second. Then, we lowered the laser power below the laser power threshold

and performed Raman mapping with a grid covering 6×40 micron². The line pattern of MoS₂ was coated with 3 nm gold and Scanning Electron Microscope (SEM) was measured with COXEM CX-200Plus, Daejeon, Korea.

For the purpose of checking the feasibility of (NH₄)₂MoS₄ becoming MoS₂, we also carried out the thermal annealing of (NH₄)₂MoS₄ crystal and its film. The thermal annealing was performed with Across International STF 1200 CVD tube furnaces system (Livingston, NJ, USA). Both (NH₄)₂MoS₄ crystals and films on glass slides were put inside a quartz tube. To avoid overpressure inside the quartz tube, the tube pressure was maintained at around 2.9 psi, which helps to create an oxygen-free environment, preventing oxidation during the annealing process. The quartz tube was passed with nitrogen gas at the flow rate of 199.9 standard cubic centimeters per minute, and the furnace was heated from room temperature to 500 °C in 50 min at the rate of 100 °C per 10 min. When the temperature reached a consistent value of 500 °C, it was maintained constant for 30 min under nitrogen gas flow. Both commercial (NH₄)₂MoS₄ and annealed samples were studied by X-ray Diffractometer (XRD) (Rigaku MiniFlex 600, The Woodlands, TX, USA).

3. Results

3.1. Conversion of (NH₄)₂MoS₄ to MoS₂ by Thermal Annealing

From now on, we use ATM for (NH₄)₂MoS₄. Before we conduct laser thermolysis, we perform the thermal annealing of ATM crystals and their film on a glass slide. Note that while we present the results for an annealed sample here, we actually study the laser thermolysis of ATM earlier. We discovered that laser power below 0.5 mW avoids the laser thermolysis of ATM and oxidation of MoS₂. Therefore, Raman spectra from the annealed samples were measured under a laser power of 0.3 mW. As shown in Figure 1a, the Raman spectrum has a strong peak at 455 cm⁻¹, as expected, for ATM crystal. After annealing, there are three peaks belonging to MoS₂: the first active Raman peak at 198 cm⁻¹ (E_{1g}), the second at 377 cm⁻¹ (E_{2g}), and the third at 408 cm⁻¹ (A_{1g}) [34]. The intensity for the peak at 198 cm⁻¹ (E_{1g}) is low. The Raman mode at 377 cm⁻¹ (E_{2g}) corresponds to out-of-plane vibrations involving only sulfur atoms and 408 cm⁻¹ (A_{1g}) is due to the opposite vibration of two sulfur atoms with respect to the molybdenum atom [34–36]. The peak at 198 cm⁻¹ belongs to MoO₂. By scanning the sample at three different locations in Figure 1b, the Raman peak at 198 cm⁻¹ does not show up in the spectrum on the purple line and is very weak in the blue line. It is possible that the laser power of 0.3 mW induced an oxidation, as discussed in more detail later.

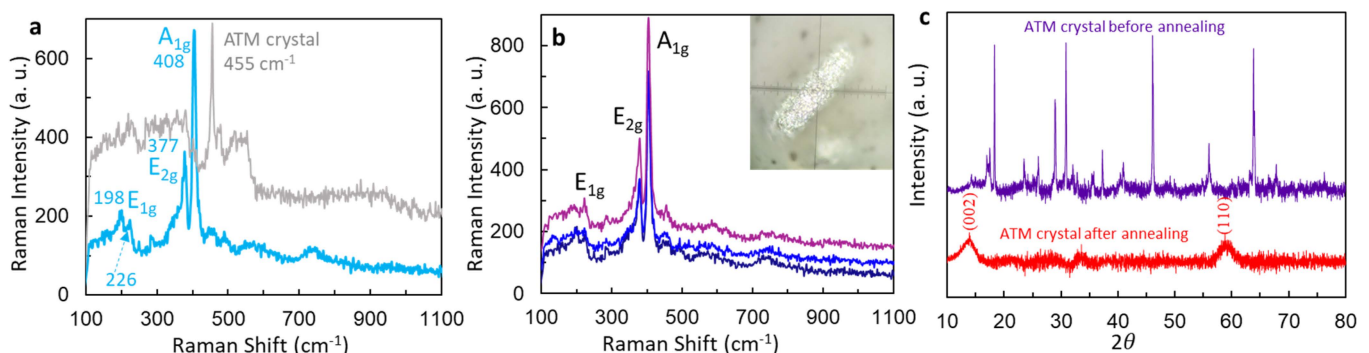


Figure 1. (a) Raman spectra at laser power 0.3 mW from ATM crystal (grey line) and from thermally annealed one (blue line) at 500 °C for 30 min. (b) Raman spectra of different Raman modes at laser power 0.3 mW from MoS₂ converted from ATM after annealing, at three different positions. (c) Comparison of XRD from ATM crystals before and after thermal annealing at 500 °C for 30 min.

The ATM crystal and annealed sample were further studied using X-ray diffraction (XRD). For the XRD from the ATM crystal in Figure 1c, the Bragg reflection peaks at $2\theta = 18.3^\circ$, 28.9° , 30.8° , and 46.1° corresponds to the crystal faces (hkl) (200), (301), (022),

and (413), respectively [22]. There are two Bragg reflection peaks at $2\theta = 14^\circ\text{C}$ and 59°C , as seen in Figure 1c, corresponding to the MoS_2 crystal of (002) and (110) [37,38]. It suggests a conversion of ATM into MoS_2 after the annealing process [37,38].

After sonication and heating at 95 degrees, the ATM film is in amorphous form as seen in the Raman spectrum as shown in Figure 2a. After the ATM film was annealed at a temperature of 500°C , the Raman spectrum in Figure 2a shows four Raman lines at 204 cm^{-1} , 226 cm^{-1} , 381 cm^{-1} , and 406 cm^{-1} for the ATM films with annellation. Again, the appearance of 204 cm^{-1} shows a trace of MoO_2 [39]. Figure 2b shows the PL spectra of exfoliated 2D MoS_2 at 10 mW and annealed ATM film under laser power at 0.3 mW. The PL for exfoliated 2D samples was measured two years ago during the study of stimulated emission [18] and reported for comparison. Both spectra look very similar in the measured wavelength range. The free exciton emission peaks A and B were observed at positions 690 nm (1.79 eV) and 630 nm (1.96 eV), respectively, for both samples [40]. Because we have observed both A and B peaks, and two peaks I_1 and I_2 related to indirect bandgap emission at position 992 nm and 883 in Figure 2b, the annealed sample from the ATM film shows multilayer MoS_2 character.

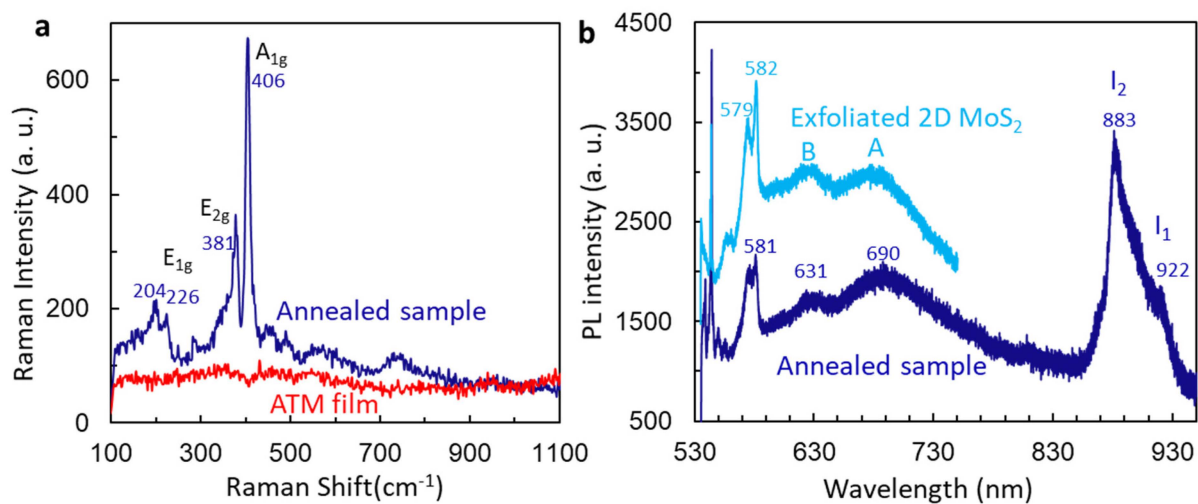


Figure 2. (a) Comparison of Raman spectra at laser power 0.3 mW from ATM film and its annealed sample. (b) PL measurement for 2D exfoliated MoS_2 under 10 mW and annealed sample from ATM film at laser power of 0.3 mW.

3.2. Laser Thermolysis of $(\text{NH}_4)_2\text{MoS}_4$ Crystals

Figure 3 shows overall Raman spectral changes taken at different laser powers ranging from 0.3 mW to 4 mW with the same integration time and at the same sample spot. At the laser power of 0.3 mW, there are two peaks at 453 cm^{-1} and 475 cm^{-1} from ATM crystal. Increasing the laser power to 0.5 mW, peaks were observed at 379 cm^{-1} , 404 cm^{-1} , 453 cm^{-1} , and 475 cm^{-1} , as shown in Figure 3a, due to a mixture of ATM and MoS_2 [38,39,41–46]. At 1 mW, the Raman signal due to ATM crystal is gone and the signal of MoS_2 becomes very weak. However, new peaks at 291 cm^{-1} , 824 cm^{-1} , and 991 cm^{-1} appear due to the formation of MoO_3 [38,39,41–46]. When the laser power goes above 1 mW, more Raman peaks related to MoO_3 appear and become stronger.

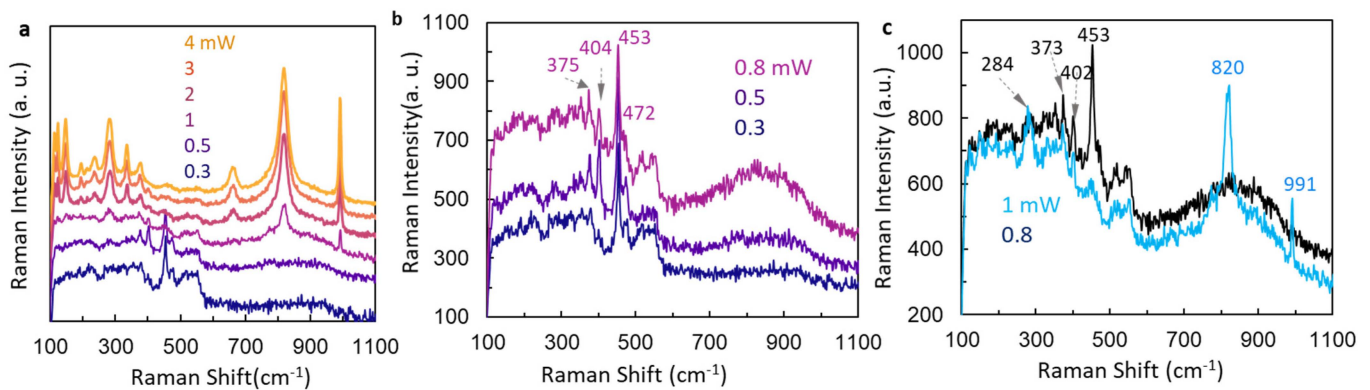


Figure 3. (a) Raman spectra from the same location of ATM crystal under laser power 0.3, 0.5, 1, 2, 3, and 4 mW. (b) Raman spectra from the same location of ATM crystal under laser power 0.3, 0.5, and 0.8 mW. (c) Raman spectra from the same location of ATM crystal under laser power 0.8 mW and 1 mW.

A more detailed examination of Raman spectra at a smaller laser power step is shown in Figure 3b,c. The Raman signal of MoS₂ at 379 cm⁻¹ and 404 cm⁻¹ appears only at 0.5 mW in Figure 3b. At 0.8 mW, the signal/ratio for the Raman peak of MoS₂ becomes worse. Raman peak at 453 cm⁻¹ is always there under these three laser powers. Increasing the laser power from 0.8 mW to 1 mW, the Raman signal at 453 cm⁻¹ disappears; thus, the sample has a mixture of MoS₂ and MoO₃. From Figure 3, we can see that the sample changes from ATM to a mixture of both ATM and MoS₂, to a mixture of MoS₂ and MoO₃, and then further to MoO₃ only with increasing laser power. Usually, MoO₂ can be converted to MoO₃ above 400 °C [39]. It means that the black-colored ATM crystal can reach a temperature above 400 °C under the CW laser photoexcitation.

3.3. Thermal Annealing and Laser Thermal Effects on Exfoliated MoS₂

In order to understand thermal annealing and laser thermal effects on MoS₂, we study the Raman spectrum of annealed samples of exfoliated MoS₂ and burned samples of MoSe₂ under the laser. Multilayer MoS₂ is very stable up to a temperature of 400 °C at atmospheric conditions. After annealing exfoliated 2D multilayer MoS₂ on a hotplate at 400 °C for 30 min, Raman modes at 286, 819, and 995 cm⁻¹ related to MoO₃ have been observed in an area without dark spots, together with E_{2g} and A_{1g} modes for MoS₂, as in Figure 4a. From our observation, oxidation of MoS₂ occurred first along the defect boundary line and at defect spots. From the defect spot with a dark color in the inset in Figure 4b, the Raman signal of MoO₂ at 199 and 224 cm⁻¹ is observed. Both MoO₂ and MoO₃ crystals can have a Raman peak at 528 cm⁻¹. However, there are four peaks in the range between 800 and 1000 cm⁻¹, at 832, 872, 918, and 936 cm⁻¹. These peaks have not been observed in MoO₂ or MoO₃. We can assign them to MoO_x. We have also observed these four Raman peaks at 833, 870, 915, and 935 cm⁻¹ in exfoliated 2D multilayer MoSe₂ excited by a laser power of 25 mW when studying the stimulated emission [47]. It seems these four peaks have nothing to do with “S” or “Se” because we observed these four peaks in both Figure 4b for MoS₂ and Figure 4c for MoSe₂.

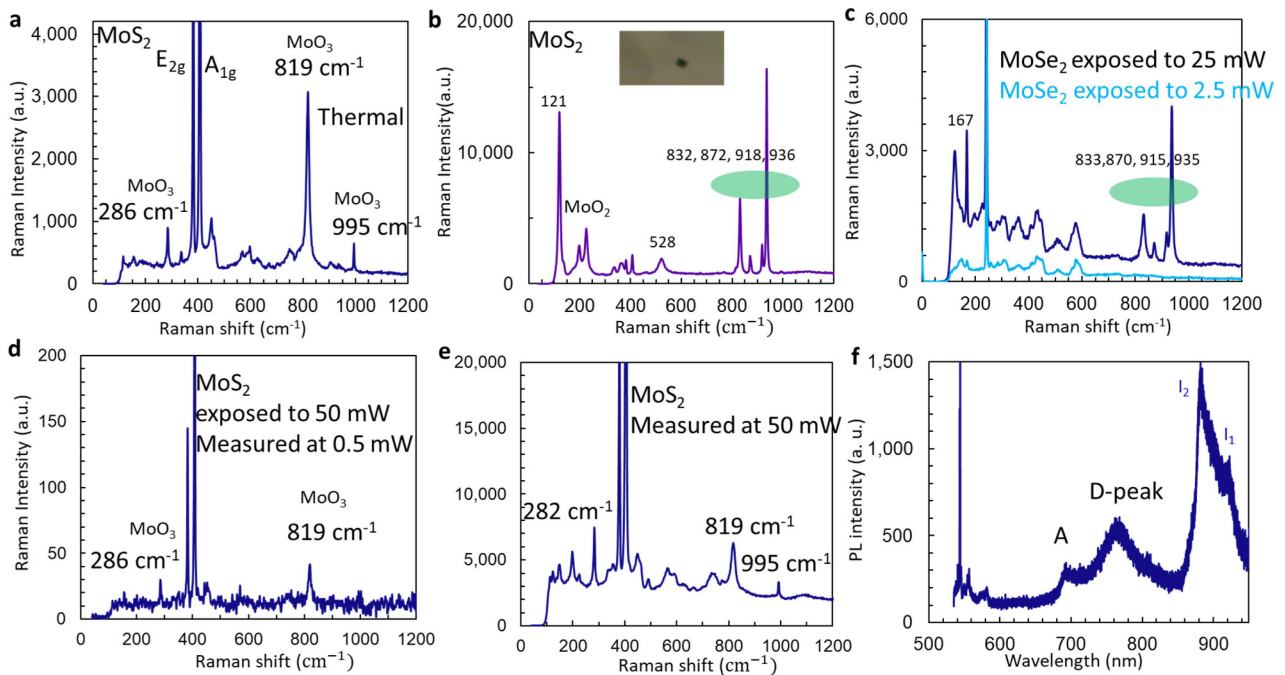


Figure 4. (a,b) Raman spectra under laser power from non-dark region (a) and dark spot ((b), image in inset) in exfoliated 2D multilayer MoS₂ annealed at 420 °C for 30 min in the atmosphere. (c) Raman spectra from exfoliated 2D multilayer MoSe₂ under laser power of 2.5 mW (light-blue line) and 25 mW (black line). (d,e) Raman spectra from exfoliated 2D multilayer MoS₂ measured at 0.5 mW after exposed to a laser power of 50 mW for 2 min (d) and measured directly under a laser power of 50 mW (e). (f) PL of exfoliated 2D multilayer MoS₂ after exposure to a laser power of 50 mW for 2 min.

After we expose the exfoliated 2D multilayer MoS₂ under a high laser power of 50 mW for 2 min using a 100× objective lens, we are able to observe two weak Raman peaks at 286 and 819 cm⁻¹ related to MoO₃, as shown in Figure 4d. When we directly measured the Raman spectrum under a high laser power of 50 mW using a 100× objective lens and 20 s integration time, we observed three Raman peaks at 286, 819, and 995 cm⁻¹ related to MoO₃ and one Raman peak around 200 cm⁻¹ related to MoO₂, as shown in Figure 4e. The weakness of the Raman signal of MoO₃ or MoO₂ might be due to the laser thinning effect [48]. The oxide is formed and becomes vapor. After exposure to high laser power, s-vacancy is formed in MoS₂ and defect peak emission [18] is seen in Figure 4f in the PL spectrum.

3.4. Laser Synthesis of MoS₂ from (NH₄)₂MoS₄ Film Using CW 532 nm Laser

After we studied and understood the laser thermolysis in ATM crystal, the thermal annealing of ATM crystal and its film, and the annealing effect of exfoliated 2D multilayer MoS₂, we can report the central piece of this publication: the laser synthesis of MoS₂.

The process started first with a set laser power for the 532 nm laser, then we exposed the sample spot to the 532 nm laser which induced laser thermolysis. This process was repeated by moving to a new location and increased the laser power for laser synthesis of MoS₂ from ATM film. Figure 5a shows Raman spectra from ATM film under a laser power of 0.5, 1, 1.5, 2, 2.5, 3, 3.5, and 4 mW. Under low excitation laser power, we did not observe the Raman peak 456 cm⁻¹ of ATM film. When the laser power goes up to 3.5 mW, several broad bands centered around 242 cm⁻¹, 343 cm⁻¹, and 460 cm⁻¹ are clearly visible. The broad bands are similar to those observed in amorphous ATM that were prepared by heating ATM at 200 °C under N₂ [45]. Our ATM preparation under sonication and thermal heating resulted in an amorphous ATM. The broad bands centered at 550 and 1100 cm⁻¹ were due to the glass substrate, as discussed later. There is a laser power threshold in the

formation of MoS₂. As seen in Figure 1a, two peaks at 376 and 402 cm⁻¹, corresponding to E_{2g} and A_{1g} modes of MoS₂, appear when the laser power goes from 3.5 to 4 mW. The difference in peak position is 26 cm⁻¹, indicating many layers of layered structure are formed in MoS₂ [23]. Although the laser was excited at different regions as shown in the inset, the laser intensity threshold behavior was confirmed using a new sample.

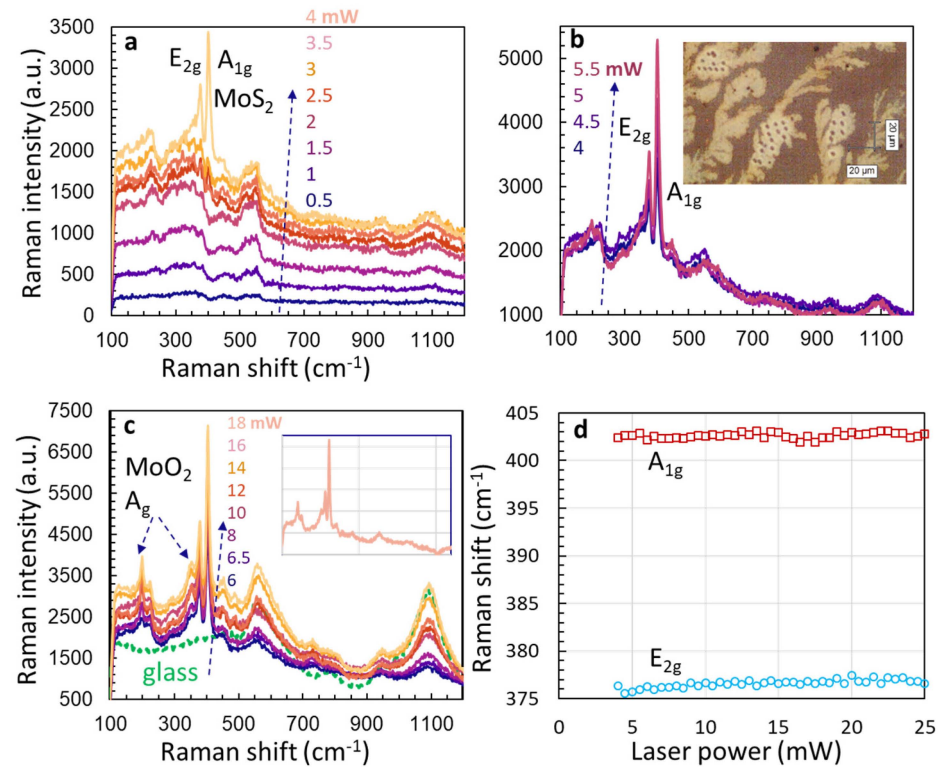


Figure 5. (a) Raman spectra from different ATM film locations under a laser power of 0.5, 1, 1.5, 2, 2.5, 3, 3.5, and 4 mW. (b) Raman spectra from different ATM locations under a laser power of 4, 4.5, 5, and 5.5 mW. (c) Raman spectra from different ATM film locations under a laser power of 6, 6.5, 8, 10, 12, 14, 16, and 18 mW. Inset is the Raman spectrum under a laser power of 18 mW after the spectrum of glass is subtracted. (d) Positions of A_{1g} and E_{2g} modes that appear from ATM film under different laser power.

The formation window of MoS₂ is narrow, as seen in Figure 5b. When the laser power is increased from 4 to 5.5 mW, a peak at 197 cm⁻¹ appears. This peak, together with a peak at 359 cm⁻¹, grows stronger when the laser power is increased from 6 to 18 mW in Figure 5c. These two peaks can be assigned to the A_g mode of MoO₂ [39]. We also measure Raman spectra from the glass substrate (dashed green line) in Figure 1c, confirming the belonging of broad bands centered at 550 and 1100 cm⁻¹ to the glass substrate. The inset in Figure 5c shows the Raman spectrum under a laser power of 18 mW after the spectrum of glass is subtracted. After the subtraction, these two broadbands are removed. There is no Raman signal of MoS₂ and MoO₃ mixture up to the laser power of 25 mW in the process of laser synthesis of MoS₂ from ATM film, as we did not observe Raman peaks at 820 and 995 cm⁻¹ (see these peaks in Figures 2 and 3) [39]. It also means that the thin ATM film has a reduced laser absorption of laser energy and the temperature of ATM film is not above 400 °C under the CW 532 nm laser photoexcitation.

Using a different sample, we then examine the Raman spectra at the same location of ATM film under different laser powers, i.e., measuring the Raman spectrum under one laser power, adjusting the laser power by increasing 0.5 mW for each step then re-measuring the Raman spectrum. When the laser power is increased from 2 to 10 mW, the Raman spectra show broad bands of amorphous ATM, as shown in Figure 6a. Again, a laser power

threshold of 10.5 mW for the appearance of E_{2g} and A_{1g} modes of MoS_2 is observed. As shown in Figure 6b, the peak intensity of E_{2g} and A_{1g} modes of MoS_2 becomes weaker with the increasing laser power from 11 to 17 mW. However, those broad bands around 550 and 1100 cm^{-1} from the glass substrate become stronger with increasing laser power, indicating that there is a photo-corrosion or laser ablation (laser thinning [48]) of thin film of ATM film and MoS_2 . We linearly normalize the Raman spectrum of glass relative to the Raman intensity of MoS_2 at a peak position near 1100 cm^{-1} and base position near 780 cm^{-1} , then calculate the subtraction as shown in Figure 6c where the broadbands are removed.

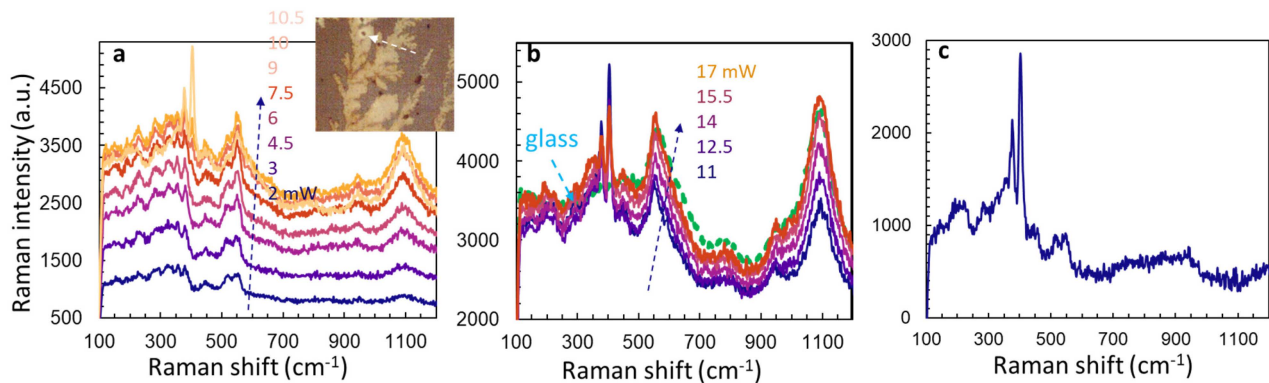


Figure 6. (a) Raman spectra from the same ATM film location under a laser power of 2, 3, 4.5, 6, 7.5, 9, 10, and 10.5 mW. (b) Raman spectra from the same ATM film location under a laser power of 11, 12.5, 14, 15.5, and 17 mW. (c) Raman spectra from the same ATM film location under a laser power of 11 mW after the normalized spectrum of glass is subtracted.

3.5. Laser Direct Writing of MoS_2 Line Pattern from $(NH_4)_2MoS_4$ Film Using CW 532 nm Laser

Through the Raman mapping program in the software, we control the laser beam to scan through in a line. Based on the experimental results in Figure 4, a threshold laser power is 4 mW for the conversion of ATM film to MoS_2 . We set a laser power of 10 mW in order to make sure we can have the laser synthesis of MoS_2 in every scanning point in the line. The optical microscope image of the scanned line by laser direct writing is shown in Figure 7a, where the line is across a region of ATM film. Then, we lowered the laser power to 1 mW, set the Raman integration to 10 s, and performed Raman mapping in a region covering that line pattern. We selected 402.5 cm^{-1} for the Raman mapping and the results are shown in Figure 7b. Clearly, only a line pattern shows the Raman signal, and other regions are dark (without the MoS_2 Raman signal). Figure 7c shows a scanning electron microscope (SEM) image of the line pattern by laser direct writing of MoS_2 from the ATM film. The line pattern is conformed in SEM. The recording resolution is close to 1.5 microns as seen from the width of the line pattern in Figure 7c.

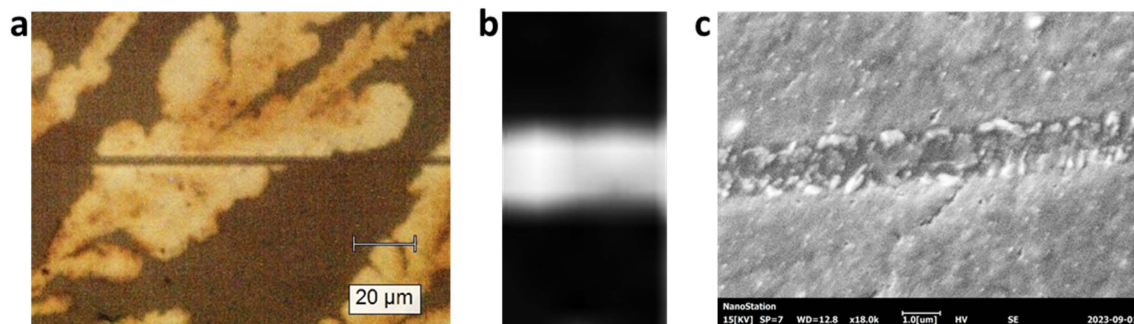


Figure 7. (a) Optical microscope image of a line pattern across an ATM film region (white area). (b) Raman mapping of the line pattern produced by the laser direct writing using a laser power of 1 mW and integration time of 10 s. (c) Scanning electron microscope image of the line pattern.

4. Discussions

The conversion of ATM to MoS₂ has been reported by other research groups [20,21]. However, we want to realize the thermolysis of ATM before we carry out the laser thermolysis. The thermal annealing of exfoliated 2D multilayer MoS₂ helped obtain the Raman feature of MoO₂ and MoO₃. The Raman peaks for MoO₃ have been observed. However, we did not observe the Raman signal of MoO₂ before the formation of MoO₃. The origin of four new Raman peaks between 800 and 1000 cm⁻¹ is still a puzzle. Because we focus on the laser synthesis of MoS₂ here, we can study their origin in the future.

Although we have achieved the laser synthesis of MoS₂ from both ATM crystal and thin film, we see a mixture of MoS₂ and ATM in the crystal sample. It is reasonable because the crystal volume is very big, while the laser thermolysis occurred in a small volume of ATM crystal. The reported laser power operation window for the laser synthesis of MoS₂ is very narrow. That operation window can be widened by changing the integration time (i.e., the exposure time for a single spot) or scanning speed if the laser direct writing method is used. On the other hand, the laser wavelength of 532 nm is near the ATM absorption edge [49]; thus, we still have an operation window for the laser thermolysis of ATM using a 50× objective lens. The absorption peak of ATM is around 470 nm [49]. The laser beam can be expanded for the thermolysis of ATM if the laser wavelength is close to 470 nm. We have not studied the film thickness-dependent laser synthesis of MoS₂. Because the change in the thickness of ATM film will modify the amount of laser energy absorption, it is feasible to achieve laser synthesis of MoS₂ from ATM film in a wide laser power window.

We did not pay attention to the ATM film quality as we focused on the capability of laser synthesis of MoS₂ using a CW laser. A uniform micropattern can be obtained using laser radiation in a high-quality film that is needed for electrical and photonic device applications. The high-quality ATM film can be achieved by mixing ATM with a polymer PEI [23,24]. For the device's capability, an ink printing method [50] can be used. The volume of ink (thus, the thickness of the film) can be precisely controlled and a desired optoelectronic pattern can be printed simultaneously followed by thermal annealing or laser thermolysis. On a high-quality film, laser direct writing [29,51] can be used for a serial fabrication of arbitrary patterns or an interference pattern of CW laser beams [31] can lead to a parallel fabrication of large-area patterns simultaneously in one exposure.

5. Conclusions

In summary, we have studied methods for the conversion of (NH₄)₂MoS₄ to MoS₂ through thermal annealing and laser thermolysis of (NH₄)₂MoS₄ crystals or film, and annealing or laser photoexcitation-induced thermal effect on exfoliated 2D multilayer MoS₂. For the first time, to the authors' best knowledge, we have realized the laser synthesis of MoS₂ from (NH₄)₂MoS₄ crystals film using a CW laser of 532 nm in a certain laser power range. There is a threshold laser power for the conversion of (NH₄)₂MoS₄ film to MoS₂. Increasing the laser power on the film has resulted in the formation of a mixture of MoS₂ and MoO₂ from the ATM film.

Author Contributions: Conceptualization, Y.L., J.C. and N.H.; methodology, Y.L., N.H., R.G.R., B.B., J.C. and B.S.; Python program, S.K.; investigation, N.H., B.B., R.G.R., B.S., S.K. and Y.L.; formal analysis, Y.L., N.H. and B.B.; writing—original draft preparation, N.H., B.B. and Y.L.; writing—review and editing, N.H., B.B., S.K., R.G.R., B.S., A.B.K., J.C. and Y.L.; funding acquisition, A.B.K., J.C. and Y.L. All authors have read and agreed to the published version of the manuscript.

Funding: This research was supported by the Department of Energy/National Nuclear Security Administration under Award Number DE-NA0004114. This report was prepared as an account of work sponsored by an agency of the United States Government. Neither the United States Government nor any agency thereof, nor any of their employees, makes any warranty, express or implied, or assumes any legal liability or responsibility for the accuracy, completeness, or usefulness of any information, apparatus, product, or process disclosed, or represents that its use would not infringe privately owned rights. Reference herein to any specific commercial product, process, or service by trade name, trademark, manufacturer, or otherwise does not necessarily constitute or

imply its endorsement, recommendation, or favoring by the United States Government or any agency thereof. The views and opinions of authors expressed herein do not necessarily state or reflect those of the United States Government or any agency thereof.

Data Availability Statement: Data will be available upon request.

Conflicts of Interest: The authors declare no conflicts of interest.

References

1. Geim, A.K.; Novoselov, K.S. The Rise of Graphene. *Nat. Mater.* **2007**, *6*, 183–191. [[CrossRef](#)] [[PubMed](#)]
2. Park, S.; Lee, A.; Choi, K.-H.; Hyeong, S.-K.; Bae, S.; Hong, J.-M.; Kim, T.-W.; Hong, B.H.; Lee, S.-K. Layer-Selective Synthesis of MoS₂ and WS₂ Structures under Ambient Conditions for Customized Electronics. *ACS Nano* **2020**, *14*, 8485–8494. [[CrossRef](#)] [[PubMed](#)]
3. Aftab, S.; Hegazy, H.H. Emerging Trends in 2D TMDs Photodetectors and Piezo-Phototronic Devices. *Small* **2023**, *19*, 2205778. [[CrossRef](#)]
4. Wang, M.; Cai, S.; Pan, C.; Wang, C.; Lian, X.; Zhuo, Y.; Xu, K.; Cao, T.; Pan, X.; Wang, B.; et al. Robust Memristors Based on Layered Two-Dimensional Materials. *Nat. Electron.* **2018**, *1*, 130–136. [[CrossRef](#)]
5. Hus, S.M.; Ge, R.; Chen, P.-A.; Liang, L.; Donnelly, G.E.; Ko, W.; Huang, F.; Chiang, M.-H.; Li, A.-P.; Akinwande, D. Observation of Single-Defect Memristor in an MoS₂ Atomic Sheet. *Nat. Nanotechnol.* **2021**, *16*, 58–62. [[CrossRef](#)]
6. Mao, J.; Wu, S.; Ding, G.; Wang, Z.; Qian, F.; Yang, J.; Zhou, Y.; Han, S. A van Der Waals Integrated Damage-Free Memristor Based on Layered 2D Hexagonal Boron Nitride. *Small* **2022**, *18*, 2106253. [[CrossRef](#)]
7. Wang, K.; Li, L.; Zhao, R.; Zhao, J.; Zhou, Z.; Wang, J.; Wang, H.; Tang, B.; Lu, C.; Lou, J.; et al. A Pure 2H-MoS₂ Nanosheet-Based Memristor with Low Power Consumption and Linear Multilevel Storage for Artificial Synapse Emulator. *Adv. Electron. Mater.* **2020**, *6*, 1901342. [[CrossRef](#)]
8. Tonndorf, P.; Schwarz, S.; Kern, J.; Niehues, I.; Del Pozo-Zamudio, O.; Dmitriev, A.I.; Bakhtinov, A.P.; Borisenko, D.N.; Kolesnikov, N.N.; Tartakovskii, A.I.; et al. Single-Photon Emitters in GaSe. *2D Mater.* **2017**, *4*, 021010. [[CrossRef](#)]
9. Aharonovich, I.; Englund, D.; Toth, M. Solid-State Single-Photon Emitters. *Nat. Photonics* **2016**, *10*, 631–641. [[CrossRef](#)]
10. Klein, J.; Sigl, L.; Gyger, S.; Barthelmi, K.; Florian, M.; Rey, S.; Taniguchi, T.; Watanabe, K.; Jahnke, F.; Kastl, C.; et al. Scalable Single-Photon Sources in Atomically Thin MoS₂. *ACS Photonics* **2021**, *8*, 669–677. [[CrossRef](#)]
11. Desai, S.B.; Madhvapathy, S.R.; Sachid, A.B.; Llinas, J.P.; Wang, Q.; Ahn, G.H.; Pitner, G.; Kim, M.J.; Bokor, J.; Hu, C.; et al. MoS₂ Transistors with 1-Nanometer Gate Lengths. *Science* **2016**, *354*, 99–102. [[CrossRef](#)] [[PubMed](#)]
12. Withers, F.; Del Pozo-Zamudio, O.; Schwarz, S.; Dufferwiel, S.; Walker, P.M.; Godde, T.; Rooney, A.P.; Gholinia, A.; Woods, C.R.; Blake, P.; et al. WSe₂ Light-Emitting Tunneling Transistors with Enhanced Brightness at Room Temperature. *Nano Lett.* **2015**, *15*, 8223–8228. [[CrossRef](#)] [[PubMed](#)]
13. Bessonov, A.A.; Kirikova, M.N.; Petukhov, D.I.; Allen, M.; Ryhänen, T.; Bailey, M.J.A. Layered Memristive and Memcapacitive Switches for Printable Electronics. *Nat. Mater.* **2015**, *14*, 199–204. [[CrossRef](#)] [[PubMed](#)]
14. Bae, S.; Kim, H.; Lee, Y.; Xu, X.; Park, J.-S.; Zheng, Y.; Balakrishnan, J.; Lei, T.; Ri Kim, H.; Song, Y.I.; et al. Roll-to-Roll Production of 30-Inch Graphene Films for Transparent Electrodes. *Nat. Nanotechnol.* **2010**, *5*, 574–578. [[CrossRef](#)] [[PubMed](#)]
15. Greben, K.; Arora, S.; Harats, M.G.; Bolotin, K.I. Intrinsic and Extrinsic Defect-Related Excitons in TMDCs. *Nano Lett.* **2020**, *20*, 2544–2550. [[CrossRef](#)] [[PubMed](#)]
16. Novoselov, K.S.; Mishchenko, A.; Carvalho, A.; Castro Neto, A.H. 2D Materials and van Der Waals Heterostructures. *Science* **2016**, *353*, aac9439. [[CrossRef](#)]
17. Choudhary, N.; Park, J.; Hwang, J.Y.; Chung, H.-S.; Dumas, K.H.; Khondaker, S.I.; Choi, W.; Jung, Y. Centimeter Scale Patterned Growth of Vertically Stacked Few Layer Only 2D MoS₂/WS₂ van Der Waals Heterostructure. *Sci. Rep.* **2016**, *6*, 25456. [[CrossRef](#)]
18. Lin, Y.; Hathaway, E.; Habis, F.; Wang, Y.; Rodriguez, R.G.; Alnasser, K.; Hurley, N.; Cui, J. Enhanced Emission from Defect Levels in Multilayer MoS₂. *Adv. Opt. Mater.* **2022**, *10*, 2201059. [[CrossRef](#)]
19. Yang, J.; Gu, Y.; Lee, E.; Lee, H.; Park, S.H.; Cho, M.-H.; Kim, Y.H.; Kim, Y.-H.; Kim, H. Wafer-Scale Synthesis of Thickness-Controllable MoS₂ Films via Solution-Processing Using a Dimethylformamide/n-Butylamine/2-Aminoethanol Solvent System. *Nanoscale* **2015**, *7*, 9311–9319. [[CrossRef](#)]
20. Samadi, M.; Sarikhani, N.; Zirak, M.; Zhang, H.; Zhang, H.-L.; Moshfegh, A.Z. Group 6 Transition Metal Dichalcogenide Nanomaterials: Synthesis, Applications and Future Perspectives. *Nanoscale Horiz.* **2018**, *3*, 90–204. [[CrossRef](#)]
21. Abbas, O.A.; Zeimpekis, I.; Wang, H.; Lewis, A.H.; Sessions, N.P.; Ebert, M.; Aspiotis, N.; Huang, C.-C.; Hewak, D.; Mailis, S.; et al. Solution-Based Synthesis of Few-Layer WS₂ Large Area Continuous Films for Electronic Applications. *Sci. Rep.* **2020**, *10*, 1696. [[CrossRef](#)] [[PubMed](#)]
22. Vinoba, M.; Navvamani, R.; Al-Sheeha, H. Controllable Thermal Conversion of Thiomolybdate to Active Few-Layer MoS₂ on Alumina for Efficient Hydrodesulfurization. *SN Appl. Sci.* **2019**, *1*, 340. [[CrossRef](#)]
23. Park, S.-W.; Jo, Y.J.; Bae, S.; Hong, B.H.; Lee, S.-K. Synthesis of Large-Scale Transition Metal Dichalcogenides for Their Commercialization. *Appl. Sci. Conver. Technol.* **2020**, *29*, 133–142. [[CrossRef](#)]

24. Yang, H.; Giri, A.; Moon, S.; Shin, S.; Myoung, J.-M.; Jeong, U. Highly Scalable Synthesis of MoS₂ Thin Films with Precise Thickness Control via Polymer-Assisted Deposition. *Chem. Mater.* **2017**, *29*, 5772–5776. [[CrossRef](#)]
25. Park, S.; Park, J.; Kim, Y.; Bae, S.; Kim, T.-W.; Park, K.-I.; Hong, B.H.; Jeong, C.K.; Lee, S.-K. Laser-Directed Synthesis of Strain-Induced Crumpled MoS₂ Structure for Enhanced Triboelectrification toward Haptic Sensors. *Nano Energy* **2020**, *78*, 105266. [[CrossRef](#)]
26. Xiong, W.; Zhou, Y.S.; Hou, W.J.; Jiang, L.J.; Gao, Y.; Fan, L.S.; Jiang, L.; Silvain, J.F.; Lu, Y.F. Direct Writing of Graphene Patterns on Insulating Substrates under Ambient Conditions. *Sci. Rep.* **2014**, *4*, 4892. [[CrossRef](#)]
27. Xiong, W.; Zhou, Y.S.; Jiang, L.J.; Sarkar, A.; Mahjouri-Samani, M.; Xie, Z.Q.; Gao, Y.; Ianno, N.J.; Jiang, L.; Lu, Y.F. Single-Step Formation of Graphene on Dielectric Surfaces. *Adv. Mater.* **2013**, *25*, 630–634. [[CrossRef](#)]
28. Wang, A.; Jiang, L.; Li, X.; Liu, Y.; Dong, X.; Qu, L.; Duan, X.; Lu, Y. Mask-Free Patterning of High-Conductivity Metal Nanowires in Open Air by Spatially Modulated Femtosecond Laser Pulses. *Adv. Mater.* **2015**, *27*, 6238–6243. [[CrossRef](#)]
29. Zuo, P.; Jiang, L.; Li, X.; Tian, M.; Xu, C.; Yuan, Y.; Ran, P.; Li, B.; Lu, Y. Maskless Micro/Nanopatterning and Bipolar Electrical Rectification of MoS₂ Flakes Through Femtosecond Laser Direct Writing. *ACS Appl. Mater. Interfaces* **2019**, *11*, 39334–39341. [[CrossRef](#)]
30. Lin, Y.; Rivera, D.; Chen, K.P. Woodpile-Type Photonic Crystals with Orthorhombic or Tetragonal Symmetry Formed through Phase Mask Techniques. *Opt. Express* **2006**, *14*, 887. [[CrossRef](#)]
31. Hurley, N.; Kamau, S.; Cui, J.; Lin, Y. Holographic Fabrication of 3D Moiré Photonic Crystals Using Circularly Polarized Laser Beams and a Spatial Light Modulator. *Micromachines* **2023**, *14*, 1217. [[CrossRef](#)] [[PubMed](#)]
32. Lutkenhaus, J.; Lowell, D.; George, D.; Zhang, H.; Lin, Y. Holographic Fabrication of Designed Functional Defect Lines in Photonic Crystal Lattice Using a Spatial Light Modulator. *Micromachines* **2016**, *7*, 59. [[CrossRef](#)] [[PubMed](#)]
33. Lee, S.; Lee, J.; Singh, J.; Rana, K.; Ahn, J. Drying-Mediated Self-Assembled Growth of Transition Metal Dichalcogenide Wires and Their Heterostructures. *Adv. Mater.* **2015**, *27*, 4142–4149. [[CrossRef](#)] [[PubMed](#)]
34. Rao, C.N.R.; Maitra, U.; Waghmare, U.V. Extraordinary Attributes of 2-Dimensional MoS₂ Nanosheets. *Chem. Phys. Lett.* **2014**, *609*, 172–183. [[CrossRef](#)]
35. Late, D.J.; Liu, B.; Matte, H.S.S.R.; Rao, C.N.R.; Dravid, V.P. Rapid Characterization of Ultrathin Layers of Chalcogenides on SiO₂/Si Substrates. *Adv. Funct. Mater.* **2012**, *22*, 1894–1905. [[CrossRef](#)]
36. Lv, R.; Robinson, J.A.; Schaak, R.E.; Sun, D.; Sun, Y.; Mallouk, T.E.; Terrones, M. Transition Metal Dichalcogenides and Beyond: Synthesis, Properties, and Applications of Single- and Few-Layer Nanosheets. *Acc. Chem. Res.* **2015**, *48*, 56–64. [[CrossRef](#)]
37. Yang, L.; Cui, X.; Zhang, J.; Wang, K.; Shen, M.; Zeng, S.; Dayeh, S.A.; Feng, L.; Xiang, B. Lattice Strain Effects on the Optical Properties of MoS₂ Nanosheets. *Sci. Rep.* **2014**, *4*, 5649. [[CrossRef](#)]
38. Wang, T.; Li, J.; Zhao, G. Synthesis of MoS₂ and MoO₃ Hierarchical Nanostructures Using a Single-Source Molecular Precursor. *Powder Technol.* **2014**, *253*, 347–351. [[CrossRef](#)]
39. de Melo, O.; González, Y.; Climent-Font, A.; Galán, P.; Ruediger, A.; Sánchez, M.; Calvo-Mola, C.; Santana, G.; Torres-Costa, V. Optical and Electrical Properties of MoO₂ and MoO₃ Thin Films Prepared from the Chemically Driven Isothermal Close Space Vapor Transport Technique. *J. Phys. Condens. Matter* **2019**, *31*, 295703. [[CrossRef](#)]
40. Mak, K.F.; Lee, C.; Hone, J.; Shan, J.; Heinz, T.F. Atomically Thin MoS₂: A New Direct-Gap Semiconductor. *Phys. Rev. Lett.* **2010**, *105*, 136805. [[CrossRef](#)]
41. Tian, H.; Roberts, C.A.; Wachs, I.E. Molecular Structural Determination of Molybdena in Different Environments: Aqueous Solutions, Bulk Mixed Oxides, and Supported MoO₃ Catalysts. *J. Phys. Chem. C* **2010**, *114*, 14110–14120. [[CrossRef](#)]
42. Jagminas, A.; Niaura, G.; Žalneravičius, R.; Trusovas, R.; Račiukaitis, G.; Jasulaitiene, V. Laser Light Induced Transformation of Molybdenum Disulphide-Based Nanoplatelet Arrays. *Sci. Rep.* **2016**, *6*, 37514. [[CrossRef](#)]
43. Ou, J.Z.; Campbell, J.L.; Yao, D.; Wlodarski, W.; Kalantar-Zadeh, K. In Situ Raman Spectroscopy of H₂ Gas Interaction with Layered MoO₃. *J. Phys. Chem. C* **2011**, *115*, 10757–10763. [[CrossRef](#)]
44. Seguin, L.; Figlarz, M.; Cavagnat, R.; Lassègues, J.-C. Infrared and Raman Spectra of MoO₃ Molybdenum Trioxides and MoO₃·xH₂O Molybdenum Trioxide Hydrates. *Spectrochim. Acta A Mol. Biomol. Spectrosc.* **1995**, *51*, 1323–1344. [[CrossRef](#)]
45. Oumahi, C.; De Barros-Bouchet, M.I.; Le Mogne, T.; Charrin, C.; Lorient, S.; Geantet, C.; Afanasiev, P.; Thiebaud, B. MoS₂ Formation Induced by Amorphous MoS₃ Species under Lubricated Friction. *RSC Adv.* **2018**, *8*, 25867–25872. [[CrossRef](#)] [[PubMed](#)]
46. Spevack, P.A.; McIntyre, N.S. Thermal Reduction of Molybdenum Trioxide. *J. Phys. Chem.* **1992**, *96*, 9029–9035. [[CrossRef](#)]
47. Lin, Y.; Hurley, N.; Kamau, S.; Hathaway, E.; Jian, Y.; Rodriguez, R.G.; Varghese, S.; Krylyuk, S.; Da-vydov, A.V.; Wang, Y.; et al. Strain-activated stimulated emission from multilayer MoSe₂ in a narrow operation window. *Phys. Status Solidi (RRL) Rapid Res. Lett.* **2024**; *in press*. [[CrossRef](#)]
48. Hu, L.; Shan, X.; Wu, Y.; Zhao, J.; Lu, X. Laser Thinning and Patterning of MoS₂ with Layer-by-Layer Precision. *Sci. Rep.* **2017**, *7*, 15538. [[CrossRef](#)] [[PubMed](#)]
49. Quagraine, E.; Georgakaki, I.; Coucouvanis, D. Reactivity and Kinetic Studies of (NH₄)₂(MoS₄) in Acidic Aqueous Solution: Possible Relevance to the Angiostatic Function of the MoS₄²⁻ Ligand. *J. Inorg. Biochem.* **2009**, *103*, 143–155. [[CrossRef](#)] [[PubMed](#)]

50. Hossain, R.F.; Bandyopadhyay, A.S.; Kaul, A.B. Vibrational Spectroscopy on Solution-Dispersed MoS₂ for Inkjet-Printed Photodetectors. *Emergent Mater.* **2022**, *5*, 477–487. [[CrossRef](#)]
51. Deubel, M.; von Freymann, G.; Wegener, M.; Pereira, S.; Busch, K.; Soukoulis, C.M. Direct Laser Writing of Three-Dimensional Photonic-Crystal Templates for Telecommunications. *Nat. Mater.* **2004**, *3*, 444–447. [[CrossRef](#)] [[PubMed](#)]

Disclaimer/Publisher’s Note: The statements, opinions and data contained in all publications are solely those of the individual author(s) and contributor(s) and not of MDPI and/or the editor(s). MDPI and/or the editor(s) disclaim responsibility for any injury to people or property resulting from any ideas, methods, instructions or products referred to in the content.